Research Article

Xingxing Lyu, Xiaosong Jiang*, Hongliang Sun, and Zhenyi Shao

Microstructure and mechanical properties of WC–Ni multiphase ceramic materials with $NiCl_2·6H_2O$ as a binder

https://doi.org/10.1515/ntrev-2020-0044
received April 25, 2020; accepted May 17, 2020

Abstract: High-density WC–Ni composite ceramics were prepared by cold isostatic pressing–vacuum pressureless sintering–hot isostatic pressing with tungsten carbide (WC) powder and $NiCl_2·6H_2O$ as a binder. Results show that with an increase in the contents of Ni in the metal binder phase, the relative density of WC–Ni composite ceramics is improved, and the formation of the carbon-deficient W_2C phase is reduced. There is no W_2C generated in the WC–1 wt% Ni material. At high temperatures, the Ni phase changes into the liquid phase and enters between the WC particles, thereby promoting the close alignment of the WC particles. Moreover, the WC particles will be more closely aligned under their own surface tension and capillary action, thereby promoting the densification of WC–Ni composite ceramics. The WC–0.5 wt% Ni composite ceramics are fully dense and show the best comprehensive performance with a microhardness of 23.0 GPa, a fracture toughness of 5.28 MPa $m^{1/2}$, and a flexural strength of 1,396.58 MPa. WC–Ni composite ceramics are mainly composed of elongated triangular prism WC particles and Ni phase. Transgranular fracture was the main fracture mode of WC–Ni multiphase ceramic materials with a small amount of intergranular fracture due to the existence of the Ni phase. Such a fracture mode can increase the flexural strength of the composite material.

Keywords: WC–Ni composite ceramics, hot isostatic pressing, densification

1 Introduction

Cemented carbides are obtained by the powder metallurgy preparation process, using a hard compound of refractory metal as the matrix and adding a transition metal (such as cobalt, nickel, and iron) as a sintering aid. WC-based cemented carbide is the most widely used cemented carbide [1–3]. Due to its excellent combination of high strength, high hardness, and high wear resistance, it is widely used in cutting tools, mining, wear parts, drilling, metal cutting, molds, and other fields [1–8]. In particular, it has excellent wear resistance and is often used in some areas with high wear resistance [9,10]. However, WC-based cemented carbides have low toughness and sinterability [11]. This is because the WC material has a hexagonal crystal structure, and carbon atoms exist in the gap of the tungsten metal lattice to form gap solid solution. The crystal structure has a strong bonding force between the WC particles, resulting in high hardness, low toughness, and low sinterability. Therefore, it is difficult to sinter densified WC materials by conventional sintering methods (such as hot press sintering and vacuum pressureless sintering (VPS)) [12].

To overcome the low sinterability and high brittleness of the WC materials, sintering aid such as Co or Fe is added into the WC particles to improve the density and toughness of the WC-cemented carbide [13]. Co is the most widely used metal binder in WC-based cemented carbides [14]. Because metal Co has excellent wettability to WC, it can reduce the sintering temperature of WC ceramics and can improve the sintering density and toughness of the material [15,16]. However, the addition of Co could decrease the hardness, wear resistance, and oxidation resistance of the WC-cemented carbides.

* **Corresponding author: Xiaosong Jiang,** Key Laboratory of Advanced Technologies of Materials, Ministry of Education, Chengdu 610031, China; School of Materials Science and Engineering, Southwest Jiaotong University, Chengdu, Sichuan 610031, China, e-mail: xsjiang@swjtu.edu.cn, tel: +86-28-87600779, fax: +86-28-87600779
Xingxing Lyu, Hongliang Sun, Zhenyi Shao: Key Laboratory of Advanced Technologies of Materials, Ministry of Education, Chengdu 610031, China; School of Materials Science and Engineering, Southwest Jiaotong University, Chengdu, Sichuan 610031, China

Thermal stress, to a large extent, limits the application of WC–Co-cemented carbides in the industrial field, which is caused by the different thermal expansion coefficients of Co and WC substrates [17,18]. In addition, Co has low reserves and costs high so that it cannot be used in a wide range [19–21]. Therefore, a growing number of researchers are striving to find a new binder to substitute Co. Studies have shown that metal Ni can be used as a binder in the sintering of cemented carbides to improve its corrosion resistance and oxidation resistance [19,20].

Results have shown that WC–Ni-cemented carbide has higher corrosion resistance and oxidation resistance than WC–Co-cemented carbide [8,22,23]. As a binder of WC-based cemented carbide materials, Ni can reduce the sintering difficulty of WC-based cemented carbide materials effectively and enables to lower the metal binder content [24,25]. This is because during the sintering process, Ni can form a liquid phase easily, which provides better wettability of WC surfaces. With the generation of the liquid-phase Ni adsorption process, the surrounding WC particles are also easily aggregated, thereby accelerating the densification of WC-based cemented carbides [26]. In addition, under vacuum sintering conditions, the liquid-phase Ni in WC–Ni cemented carbide increases as the temperature increases. An increase in the liquid-phase Ni accelerates the movement of WC particles and, on the other hand, promotes its homogeneous distribution around WC particles, expediting the densification process. Finally, an almost completely densified WC–Ni cemented carbide material is obtained [3]. In the actual industrial production, Ni is lower in costs than Co and the storage amount of Ni is much larger; hence, it is a better choice to use Ni instead of Co as the bonding phase of the cemented carbide [27].

However, the commonly used nickel binders for preparing WC–Ni multiphase ceramics are nickel powder and nickel oxide powder. After the addition of nickel oxide powder, the appearance of nickel pool is easy after the mechanical alloying treatment [28,29]. Therefore, this article hopes to find a source of Ni that can be dissolved in water or alcohol solvents and then attempts to use $NiCl_2{\cdot}6H_2O$ as the source of Ni. This is because $NiCl_2{\cdot}6H_2O$ has the advantage of being easily soluble in water; hence, it is not easy to agglomerate in the ball mill to avoid the nickel pool phenomenon. Therefore, in this article, $NiCl_2{\cdot}6H_2O$ was used as the sintering aid, and after ball milling with WC powder, WC–Ni composite ceramics were prepared by cold isostatic pressing–vacuum pressureless sintering (VPS)–hot isostatic pressing (HIP) densification technology. The three different Ni addition amounts (0.25, 0.5, and 1 wt%) of WC–Ni composite ceramics were vacuum sintered at 1,530 and 1,560°C, then subjected to HIP. Microstructure properties were characterized and analyzed. And the strengthening and toughening mechanisms of experimental WC–Ni composites were discussed.

2 Experimental procedure

2.1 Material preparation

In this experiment, ultrafine WC powder (Xiamen Jinlu Special Alloy Co., Ltd, 0.53 μm, containing a small amount of VC and Cr_3C_2) and $NiCl_2{\cdot}6H_2O$ powder (Chengdu Kelong Chemical Reagent Factory, Analytical Grade) were used as raw materials. $NiCl_2{\cdot}6H_2O$ was used as the Ni source to substitute Co as a metal binder, and the composition of the design specimens having different Ni contents is given in Table 1.

Table 1: WC–Ni composite ceramics raw material powder content

Numbering	Ingredient	WC (wt%)	Ni (wt%) ($NiCl_2{\cdot}6H_2O$)
WCN-1#	WC–0.25 wt% Ni	99.75	0.25
WCN-2#		99.75	0.25
WCN-3#	WC–0.5 wt% Ni	99.50	0.50
WCN-4#		99.50	0.50
WCN-5#	WC–1 wt% Ni	99.00	1.00
WCN-6#		99.00	1.00

The main experimental steps are shown in Figure 1. The raw material powder was placed in a planetary ball mill (DECO-PBM-AD-2; Changsha Deco Instrument Equipment Co., Ltd) for 2 h to make the mixture uniform. The ball-milled raw material was then dried in a freeze dryer (FD-1B-50; Beijing Bo Medical Laboratory Instrument Co., Ltd) for 24 h to obtain a dried mixed powder. The mixed powder was pressed into a cylindrical piece with a diameter of 30 mm, and a total of six specimens were designated as WCN-1#, WCN-2#, WCN-3#, WCN-4#, WCN-5#, and WCN-6#. The press-formed sheet specimen was placed in a plastic wrap to vacuum and then placed in a cold isostatic pressing tester (LDJ600-200-300; Chuanxi Machinery Factory) for 10 min at the pressure of 200 MPa. The cold isostatically pressed specimen was sintered in a vacuum hot press sintering furnace (VTP-1; Shenyang Weitai technology) according to the process given in Table 2. After that, the specimens were placed in an HIP furnace (QIH-15, ABB, USA) and sintered without encapsulation in an Ar gas

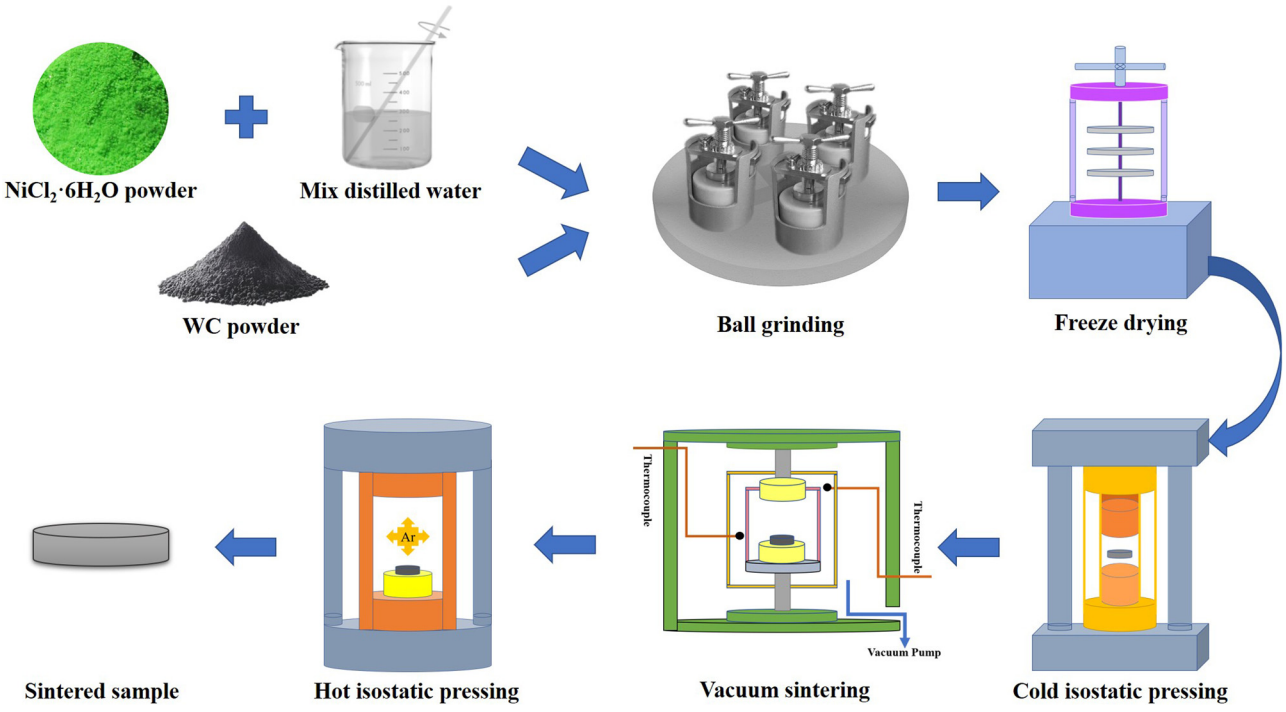

Figure 1: Flow chart of the experimental specimen preparation.

medium; the temperature, pressure, and time were set according to the data given in Table 2.

2.2 Material characterization

The densities of WC–Ni composite ceramic materials were measured by the Archimedes method, and the phase composition of the composites was analyzed using X-ray diffraction (XRD; Philips PM1700). The hardness tester (HV-50 Vickers) was used to test its Vickers hardness, the load was 10 kg, and the dwell time was 15 s; each specimen is measured 5 points to average. The indentation method was used to measure the fracture toughness of the composite, and the flexural strength of the composite was characterized by the three-point bending test (WDW-3100 Microcomputer Controlled Electronic Universal Material Testing Machine). The microstructure, fracture morphology, and interface bonding of the composites were observed by scanning electron microscopy (SEM; FEI Inspect F50) and transmission electron microscopy (TEM; FEI Titan G2 60-300). The compositions and elemental distributions of the composites were analyzed using an energy dispersive X-ray spectrometry (EDS; FEI Inspect F50).

3 Experimental results

3.1 Composition and microstructure of mixed powders

Figure 2(a) shows the XRD pattern of the WC powder before ball milling and the XRD pattern of the mixed

Table 2: WC–Ni composite ceramics sintering process

Numbering	Ingredient	Sintering process	HIP
WCN-1#	WC–0.25 wt% Ni	VPS 1,530°C × 1.5 h	1,600°C × 80 MPa × 1 h
WCN-2#		VPS 1,560°C × 1.5 h	1,600°C × 80 MPa × 1 h
WCN-3#	WC–0.5 wt% Ni	VPS 1,530°C × 1.5 h	1,600°C × 80 MPa × 1 h
WCN-4#		VPS 1,560°C × 1.5 h	1,600°C × 80 MPa × 1 h
WCN-5#	WC–1 wt% Ni	VPS 1,530°C × 1.5 h	1,600°C × 80 MPa × 1 h
WCN-6#		VPS 1,560°C × 1.5 h	1,600°C × 80 MPa × 1 h

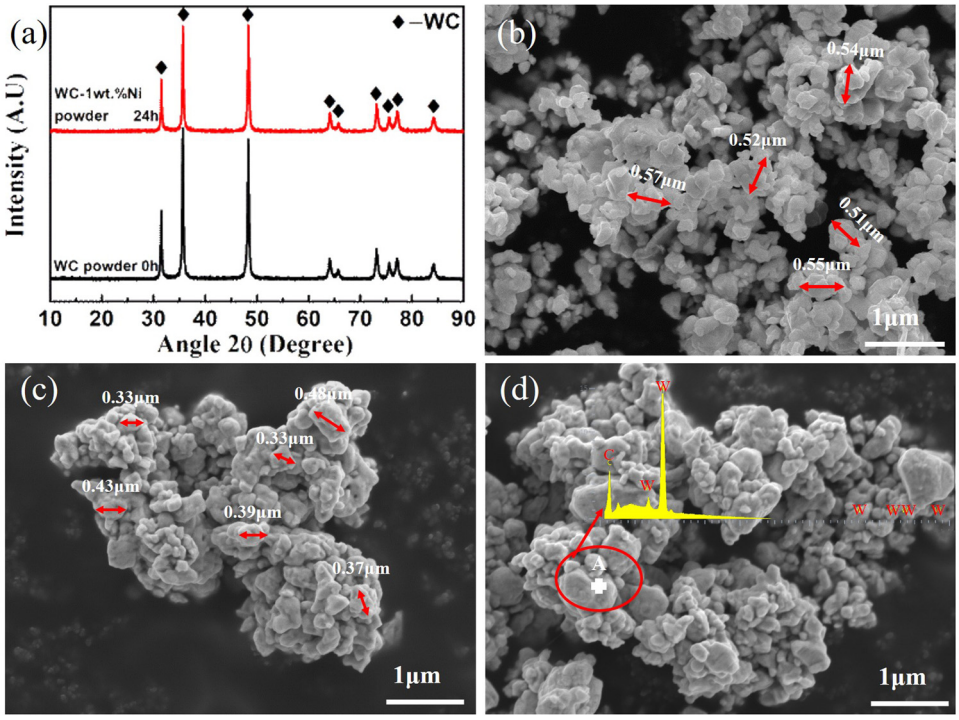

Figure 2: (a) XRD patterns of the WC–1 wt% Ni composite powders ball milled at different times, (b) SEM images of the WC power, (c) SEM images of the WC–1 wt% Ni powder, and (d) EDS images of WC–1 wt% Ni powder.

powder after adding $NiCl_2{\cdot}6H_2O$ and ball milling with WC powder for 24 h. It is found that after 24 h of ball milling, the diffraction peak of WC weakened and cracked, indicating a decrease in the crystal size [30–32]. No diffraction peak of Ni was detected because of its low content. Figure 2(b) and (c) shows the SEM images of the WC powder and the WC–1 wt% Ni powder, respectively, and the particles show a polyhedral shape. The average particle size of the WC powder is 0.53 μm, which was obtained by the line intercept method, and the average particle size of WC–1 wt% Ni powder is 0.39 μm. It can be seen that the particle size of the powder after ball milling is reduced. The ball mill makes the powder more uniform, which laid a good foundation for postsintering densification.

3.2 Phase composition and microstructure of WC–Ni composite ceramics

Figure 3 shows the XRD patterns of six specimens at different compositions after different sintering processes. According to the XRD pattern analysis, it can be observed that the main diffraction peaks belong to the WC phase, whereas all specimens sintered by vacuum contain a small amount of W_2C. In Figure 3, the Ni content in each of the two groups increased from top to bottom sequentially. Conversely, the intensity of the diffraction peak of the carbon-deficient phase W_2C gradually decreased and almost disappeared. The occurrence of W_2C was due to its great relationship with the sintering temperature and holding time; the carbon-deficient phase WC_{1-x} is easier to generate at high temperatures and long holding time. In addition, as a small amount of oxide layer or oxygen was adsorbed on the surface of the raw powders, it would react with graphite at high temperatures and long holding time to make the stoichiometric ratio of W to C greater than 1; thus, W_2C phase was formed during the sintering process. In Figure 3(e) and (f), when the Ni content is 1 wt%, only the WC phase diffraction peak is present in the specimen and the carbon-deficient phase W_2C substantially disappears. In this work, since the WC–Ni multiphase ceramics were studied with less binder phase, the Ni content in the specimen material is at a quite low level; hence, no Ni phase diffraction peaks were found [28]. It can be seen from the spectrum that the W_2C content of the carbon-deficient phase decreases with an increase in the Ni content, and the W_2C diffraction peak intensity of the carbon-deficient phase in the specimen sintered at 1,560°C is lower than that of

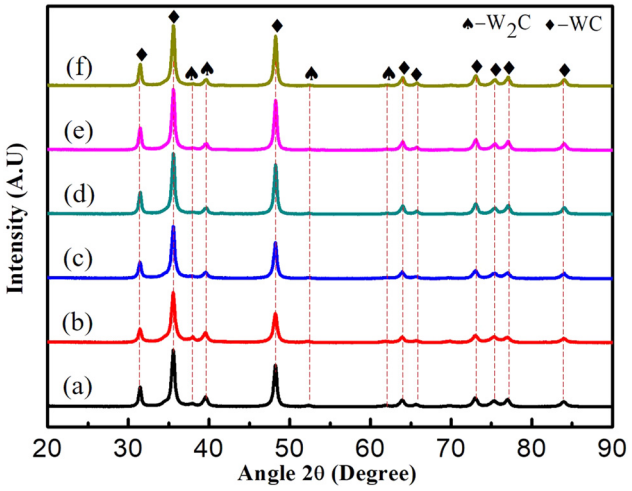

Figure 3: X-ray diffraction pattern of the WC–Ni composite ceramic specimen: (a) WCN-1#, (b) WCN-2#, (c) WCN-3#, (d) WCN-4#, (e) WCN-5#, and (f) WCN-6#.

the specimen with the same Ni content. It indicates that the more carbon-deficient the phases, the lower the density of the material [33].

According to the analysis of the raw material powder, the carbon content in the raw material powder satisfies the stoichiometric ratio but contains 0.29 wt% of oxygen. The presence of W_2C may be due to the reduction of oxides on the surface of the powder during sintering, thereby consuming C in the powder, making it impossible to maintain the stoichiometric ratio required to form WC [34]. Besides, the raw material powder was exposed to vacuum and reducing atmosphere in the graphite mold. At a high temperature, the surface oxide may also be reduced by C in the mold or the generated CO to form W powder, so that the atomic ratio of W to C is greater than 1, thereby forming W_2C. In addition, when referring to the W–C binary phase diagram [35], the phase behavior of the (W_2C + WC) state is exhibited at a sintering temperature higher than 1,250°C. During the sintering process, α–W has a relatively low activation energy (Q_v = 247 kJ/mol) and tends to form a W_2C phase by C diffusion reaction with $2W + C \rightarrow W_2C$. Second, the formation of W_2C may be achieved by rapid cooling of the WC, which is formed by temperature-driven, non-equilibrium transitions for kinetically advantageous products such as W_2C and WC_{1-x} [36,37]. This also explains the presence of W_2C in the specimen. The W_2C (content less than 3.5 wt%) in WC ceramics has little effect on hardness and fracture toughness, but when the content of W_2C increases to a certain extent, its hardness and fracture toughness decrease significantly with an increase in the W_2C content [33].

Figure 4 presents the backscattered topography and EDS elemental surface distribution of the specimenWCN-6#. The gray matrix in Figure 4(a) corresponds to WC, and the Ni element distribution is very uniform (Figure 4(c)–(e)), and no agglomerate of Ni is present [28].

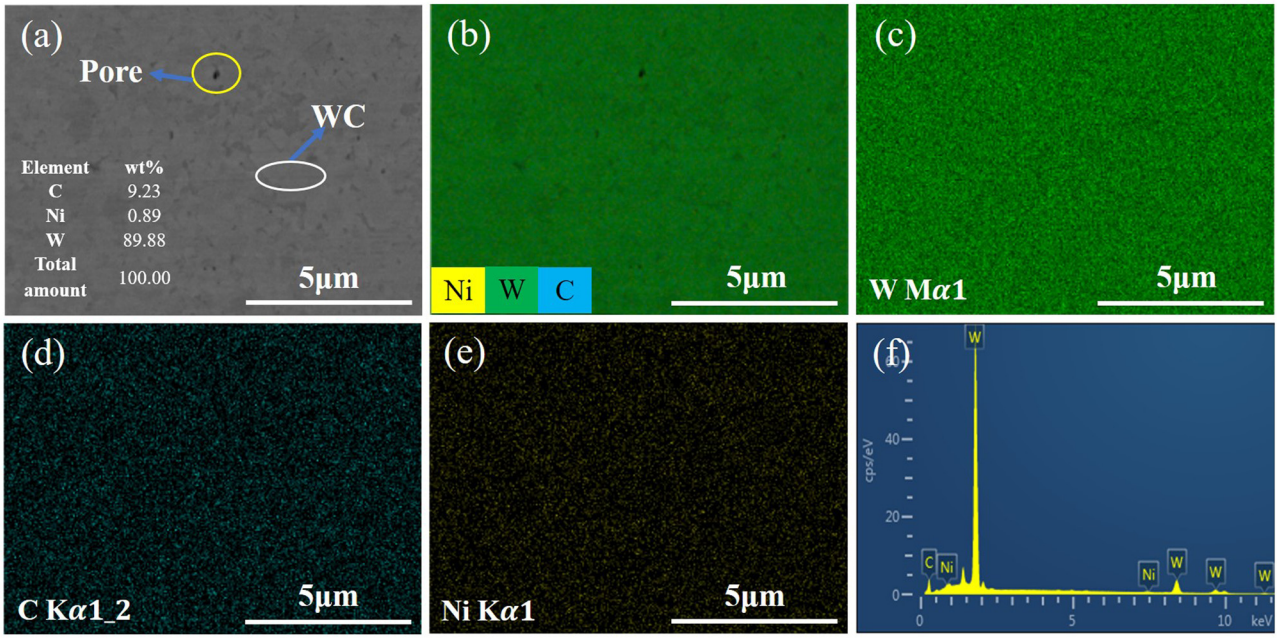

Figure 4: WCN-6# backscatter topography and surface scanning map, (a) backscatter topography, (b) surface scanning map, (c) Element W, (d) Element C, (e) Element Ni, and (f) EDS results.

During high-temperature sintering, the Ni phase adhesive becomes a liquid phase to make the densification easier, and the void defects that generate after high-temperature sintering can sufficiently grind the powder particles during mixing, reducing aggregation and making the specimen more compact after sintering. Since Ni belongs to the FCC crystal system and has good plasticity, it is easy to deform plastically during the wet grinding process to form a sheet-like Ni powder mass. Therefore, it is necessary to avoid the aggregation effect of the powder during wet grinding, so that the phenomenon of "nickel pool" can be eliminated. Increasing the sintering temperature or prolonging the holding time and HIP can reduce the porosity and improve the overall performance of the cemented carbide [3,26].

Figure 5 shows a transmission electron microscopic analysis of the specimen WCN-4#. It can be seen from Figure 5(a) that the WC grain morphology is mainly lath and triangular, which is because the WC monomorphism tends to be in triangular prism shape, so the crystal grains appear as triangles and slats [38]. The intrinsic factor that determines the grain morphology is determined by the point group. It can be seen that the space group of WC is $P\bar{6}m2$, and the space group knows that the point group of WC is $\bar{6}m2$, and the lattice constant a in a WC unit cell is greater than c [39]. Based on the relation among the point group, the initial surface, and the simple shape, when the initial surface is $(10\bar{1}0)$, the simple shape of the WC is a triangular prism, the shape of the predicted WC grain is a strip shape, and the initial surface is (0001). When the WC has a simple shape on both sides, the predicted WC grain shape is a triangle. The crystallographic plane reflects the anisotropy of the crystal, which is caused by the different surface energies of the crystal faces. The WC grains are lath-like because the surface energies of $(01\bar{1}0)$ and (1000) are different [28,40,41]. Figure 5(b) shows the electron diffraction

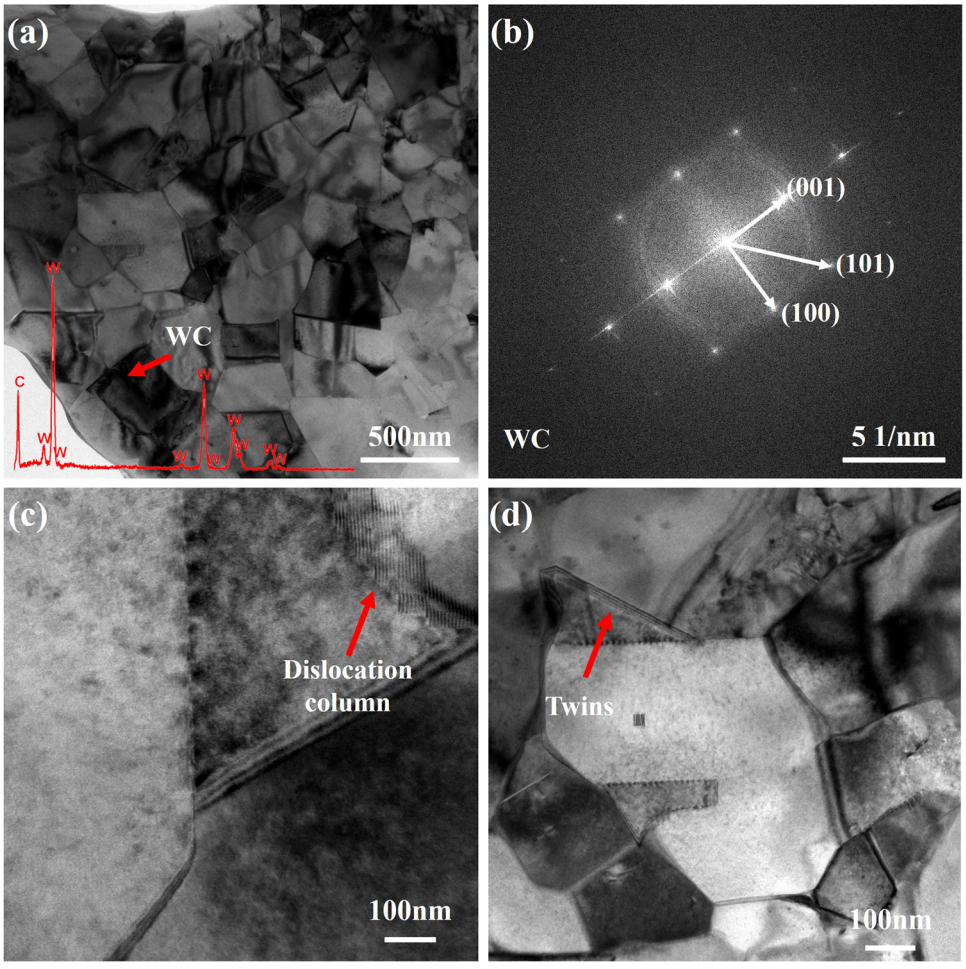

Figure 5: WC grain morphology and corresponding electron diffraction pattern of WCN-4# specimen and crystal defects of specimen: (a) WC grain morphology, (b) electron diffraction pattern of WC grain, (c) dislocation column, and (d) twins.

pattern of the WC grain in specimen WCN-4#, inferring that the grain only contains WC and its crystal axis direction is [010]. Figure 5(c) and (d) shows the crystal defects in specimen WCN-4#. A large number of crystal defects such as dislocation arrays and twins can be observed in the WC crystal grains. In Figure 5(c), the parallel distribution of dislocations can be seen. The observed twin morphology is shown in Figure 5(d). It can be seen from the figure that the twins are almost parallel and the interface is straight grid interface. The information of dislocation column may be due to high temperature and high pressure, the crystal grains are plastically deformed, the dislocations are proliferated, and these dislocations slide down in the force. When the obstacles are encountered, they are plugged in front of the obstacles. Delivery may occur when the wrong encounter occurs. When the dislocation moves to the grain boundary, the motion of the dislocation is blocked, and it will be concatenated near the grain boundary, thereby forming a dislocation column [28]. Due to the existence of dislocation columns, the dislocations of WC grains are difficult to slip at room temperature, stress concentration is easily formed in the crystal grains, and the stress concentration caused by each crystal grain is different, so the crystal defects are distributed uniformly. It may be one of the reasons why the dispersion of the flexural strength is large.

Figure 6 shows a transmission electron microscopic analysis of WC, Ni, WC, and Cr_3C_2 performed on the specimen WCN-4#. It can be seen from Figure 6(a) that the nickel phase is mainly distributed at three points in the boundary, the volume is relatively small, and the distribution is uniform, and no agglomeration occurs. Figure 6(a) shows that the nickel phase diffuses in this region, which is consistent with the characteristics of liquid phase sintering. At high temperatures, the nickel phase becomes liquid and rapidly permeates into the pores between the WC particles. The nickel phase has good wettability and will cover the WC particles well; hence, the nickel phase can be well distributed at the

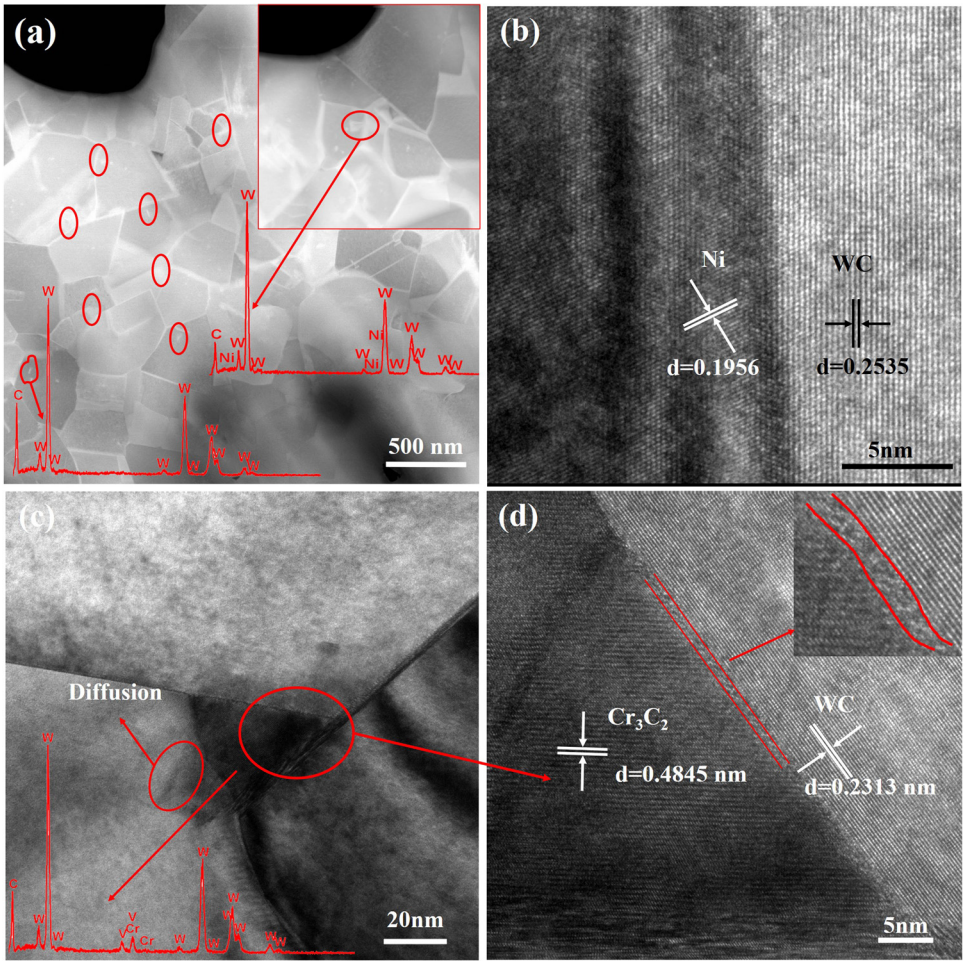

Figure 6: (a) TEM results of the topography, (b) TEM results between WC and Ni, and (c and d) TEM results between WC and Cr_3C_2.

grain boundaries [28,42]. Figure 6(b) shows an interface diagram of WC and Ni. It can be seen that WC and Ni are well combined, and the interplanar spacing of Ni phase and WC is 0.1956 nm and 0.2535 nm, respectively. TEM (Figure 6(c)) and EDS (Figure 6(d)) were used to observe and analyze the distribution of grain growth inhibitors VC and Cr_3C_2. Figure 6(c) shows the typical microscopic morphology and corresponding energy spectrum at the triple grain boundary. It could be observed that the grain boundary at this point is a flat grain boundary where V and Cr are detected. Analysis shows that there are grain growth inhibitors VC and Cr_3C_2. Figure 6(d) shows a high-resolution diagram of WC and Cr_3C_2. The interplanar spacing of WC and Cr_3C_2 is 0.2313 and 0.4845 nm, respectively, and it is found that Cr_3C_2 is diffused, which better limits the growth of WC grains. It is found that the flat grain boundary is a rough interface on the atomic scale, and the facet grain boundary is a smooth interface on the atomic scale. When the grain boundary is straight, the grain grows normally. However, when the grain boundary is a facet, it will cause grain growth abnormally [12,43]. Therefore, when the grain inhibitors VC and Cr_3C_2 are added, VC and Cr_3C_2 will hinder the growth of grains under high temperature and long-term sintering conditions; hence, fine microstructures can still be obtained. Therefore, the density and fracture toughness of WC–Ni composite ceramics can be improved [42,44]. In addition, VC and Cr_3C_2 at the grain boundaries can reduce the surface energy of WC particles and reduce the driving force for the grain growth [45].

3.3 Performance analysis of WC–Ni composite ceramics

3.3.1 Density

When compared with the conventional method, the preparation method in this paper uses $NiCl_2{\cdot}6H_2O$ as the nickel source. This is because $NiCl_2{\cdot}6H_2O$ has the advantage of being easily soluble in water; hence, it is not easy to agglomerate in the ball mill to avoid the nickel pool phenomenon. The appearance of the nickel pool will greatly reduce the density and mechanical properties of WC–Ni composite ceramics. Therefore, avoiding the appearance of the nickel pool is of great significance to the density and mechanical properties of WC–Ni composite ceramics. As shown in Figure 7, the densities of the WC–Ni composite ceramic materials of different compositions and different sintering processes

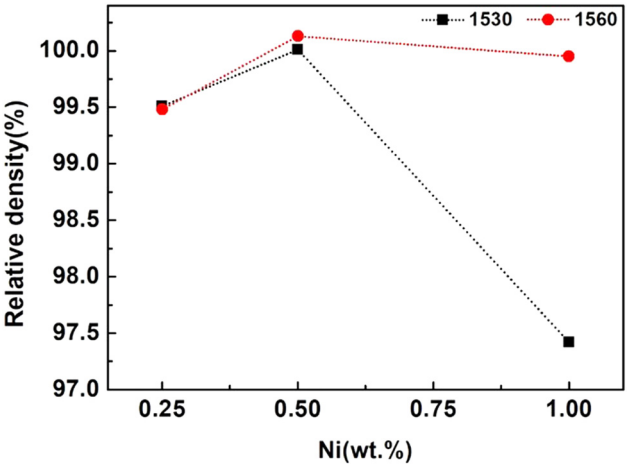

Figure 7: WC–Ni composite ceramics density.

generally show a tendency to increase with an increase in the Ni content. It can be seen that the adhesive Ni exhibits a good promotion effect on the sintering densification of the WC–Ni composite ceramic material. That is because Ni can be easily melted into a liquid phase at a high temperature and penetrates the pores between the WC particles so that the WC particles can be well infiltrated and the WC particles are more closely arranged under the action of surface tension and capillary effect at this time to increase the density of the specimen [26]. At the same time, as the sintering temperature increases, both the fluidity of liquid Ni and the driving force of sintering increase, which accelerates the densification of ceramic materials and increases the density of ceramic materials. From the results of the specimen densification of WC–Ni composite ceramics with 0.25, 0.5, and 1 wt% Ni metal binder phases after VPS at 1,530 and 1,560°C and then HIP, the analysis shows that WCN-4#, the ceramic material of WC–0.5 wt % Ni sintered at 1,560°C, has the best densification degree, reaching 100.13%, indicating that the material is completely dense. The relative density is greater than 100% because of the reaction occurring during the sintering process, which provides a phase different from that of the original material; hence, the density theoretically obtained by the mixing rule is not the best reference for the relative density or is obtained from the density value porosity data [46]. WC–0.25 wt% Ni and WC–1 wt% Ni specimens have a density lower than WC–0.5 wt% Ni specimen. Comparing the densities of ceramic specimens at different sintering temperatures of the same composition, it can be found that the WC–Ni composite ceramic specimens sintered at 1,560°C are denser than that of the vacuum sintered WC–Ni ceramic

specimens at 1,530°C. On the whole, the densities of 0.25, 0.5, and 1 wt% of the composite materials of Ni content are more than 97%, and the degree of densification is greatly improved when compared with pure WC ceramics. The main reason is that the VPS process makes the material dense, then the HIP treatment can make the material completely dense, and the density is increased to achieve secondary densification. The density of the specimen WCN-5# in the data was significantly reduced, probably due to an increase in the Ni content, which led to a longer period of liquid phase sintering, resulting in a decrease in the density. At the same time, Lisovsky [47] found that the flow driving force of the binder liquid phase between the WC particles is inversely proportional to the WC particle size. Therefore, the rearrangement of the WC particles in the liquid phase could be accelerated as the sintering temperature and the binder increase, and at the same time, the growth of the WC particles could also be promoted. Therefore, the flow driving force of the binder liquid phase between the WC particles is reduced, resulting in a decrease in the driving force of the binder liquid phase filling hole and a decrease in the density.

3.3.2 Hardness and fracture toughness

Table 3 presents the mechanical property results of WC–Ni composite ceramic materials with different binder contents (0.25, 0.5, and 1 wt%). It can be seen from Figure 7 that Ni has a significant influence on WC sintering to achieve high density. When the Ni content is 0.25 wt%, the hardness, fracture toughness, and flexural strength of specimen WCN-2# are 23.90 GPa, 4.10 MPa $m^{1/2}$, and 935.87 MPa, respectively. As the Ni content increased to 1 wt.%, the hardness, fracture toughness, and flexural strength of specimen WCN-6# are 23.00 GPa, 4.30 MPa $m^{1/2}$, and 1514.77 MPa, respectively. This shows that an increase in the Ni content greatly improves the flexural strength of WC–Ni composite ceramics [28]. At the same time, WC–Ni composite ceramic materials have a high hardness of more than 21.0 GPa, which is significantly higher than the WC–15 wt % Co composite (less than 17 GPa) prepared by Shih-Hsien Chang [48] and is close to fully dense (approximately 24 GPa) pure WC prepared by other researchers [18,49]. When the sintering temperature is 1,560°C, the hardness of the WC–Ni composite ceramics specimen decreases with an increase in the Ni content, which is due to the increase in the Ni content, which leads to a longer period of liquid phase sintering, resulting in a decrease in the density. At the same time, the flow driving force of the binder liquid phase between the WC particles is inversely proportional to the WC particle size. Therefore, with an increase in the sintering temperature and the binder, the rearrangement of WC particles in the liquid phase is accelerated, and the growth of WC particles is promoted. Due to the growth of WC particles, this hinders the flow of the binder liquid phase and reduces the driving force for the binder liquid phase to fill the pores, resulting in the presence of pores between the WC particles, which can reduce the density and hardness [47].

In this work, the fracture toughness test of the indentation method [50] was used. The K_{IC} calculation formula is calculated by the indentation method:

$$K_{IC} = 0.075P{\cdot}C^{-3/2}, \tag{1}$$

where K_{IC} is the fracture toughness (kgf $m^{-3/2}$), P is the load size (kgf), and C is the diagonal length of indentation crack (mm), as 1 kgf $m^{-3/2}$ = 0.31 MPa $m^{1/2}$, hence it can be converted to

$$K_{IC} = 0.02325\ P{\cdot}C^{-3/2}, \tag{2}$$

where K_{IC} is the fracture toughness (MPa $m^{1/2}$), P is the load size (kgf), and C is the diagonal length (mm) of indentation crack.

Figure 8 compares the hardness and fracture toughness of each group of the WC–Ni composites. Observing and analyzing the fracture toughness data

Table 3: Performance of WC–Ni composite ceramics

Numbering	Ingredient (wt%)	Hardness (GPa)	Fracture toughness K_{IC} (MPa $m^{1/2}$)	Bend-resistant strength (MPa)
WCN-1#	WC–0.25 wt% Ni	22.50(±0.22)	5.76(±0.37)	1168.29(±246.28)
WCN-2#		23.90(±0.22)	4.10(±0.21)	935.87(±272.03)
WCN-3#	WC–0.5 wt% Ni	21.83(±0.05)	4.14(±0.22)	1225.06(±139.24)
WCN-4#		23.00(±0.22)	5.28(±0.25)	1396.58(±50.17)
WCN-5#	WC–1 wt% Ni	23.73(±0.12)	4.38(±0.28)	1181.17(±105.51)
WCN-6#		23.00(±0.12)	4.30(±0.09)	1514.77(±259.6)

and the graph, it is known that the fracture toughness of WC–Ni composite ceramics specimens decreases first and then increases with an increase in Ni content at a sintering temperature of 1,530°C, but in the WC–Ni complex phase at a sintering temperature of 1,560°C, the fracture toughness of ceramic specimens increases first and then decreases with an increase in the Ni content; hence, the Ni content and sintering temperature will affect the fracture toughness at the same time. Moreover, the W_2C existing in WC ceramics has an effect on the hardness and fracture toughness. It is found that the hardness and fracture toughness of WC ceramics decrease with an increase in the W_2C content [33]. According to the XRD phase analysis, it can be known that an increase in the Ni content makes the content of carbon-deficient phase W_2C gradually decrease or even disappear. The decrease of carbon-deficient phase W_2C is beneficial to improve the density and performance of the material; hence, the fracture toughness of the material gradually increases. When the Ni content increases from 0.25 to 0.5 wt%, the fracture toughness increases [33]. When the content of Ni in the metal binder phase is 0.25 wt% sintering at 1,560°C, the WC–Ni composite has the highest hardness of 23.9 GPa and fracture toughness of 4.10 MPa $m^{1/2}$. The fracture toughness of the WC–Ni composite prepared by sintering at 1,530°C is as high as 5.76 MPa $m^{1/2}$, and the hardness of the material is also high (22.5 GPa).

3.3.3 Flexural strength

Figure 9 shows the flexural strength of each group of the WC–Ni composites. The flexural strength of the specimen generally increases with an increase in the Ni content. Since the uniformity and continuity of the microstructure of the material will affect the flexural strength of the material, the addition of an appropriate amount of Ni makes the WC grain size more uniform, so that the flexural strength of the WC–Ni composite ceramics is improved while it is easy to cause aggregation due to the excess Ni. Specimen WCN-2# has the lowest flexural strength value of 935.87 ± 272.03 MPa even though the sintered WC–Ni composite ceramic at 1,560°C has a lower density. In contrast, specimen WCN-6# with the WC–Ni composite ceramics sintered at 1,560°C has a flexural strength of 1514.77 ± 259.6 MPa, which is due to better liquid phase sintering results [14]. As can be seen from Figure 7, when the sintering temperature is from 1,530 to 1,560°C, the relative density of the WC–Ni multiphase ceramics exceeds 99%. In general, the internal pores of the material are prone to stress concentration. However, the WC–Ni composite ceramics sintered at 1,530 and 1,560°C achieve almost complete densification, which effectively reduces the strain point along with the fracture mechanism and increases the resistance bend strength value. At the same time, the improvement of the Ni phase contributes to the densification of the samples, and sintering at high temperatures generates a large amount of liquid phase filling the pores [51,52], which also greatly improves the flexural strength of the WC–Ni composite ceramics.

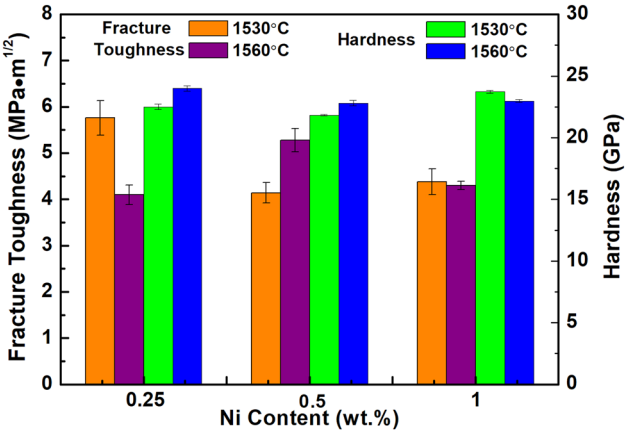

Figure 8: Hardness and fracture toughness of each specimen of WC–Ni composite ceramics.

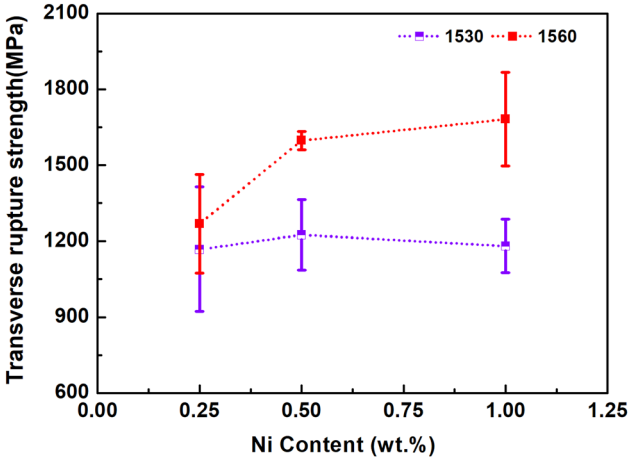

Figure 9: Flexural strength of each specimen of WC–Ni composite ceramics.

4 Discussion

4.1 Densification mechanism

For WC-based cemented carbides, WC grain growth is divided into two stages during the sintering densification process. The first is a solid phase sintering stage in

which small WC particles are grown by surface diffusion to contact with each other. The second is a liquid phase sintering stage in which small WC particles are premelted due to the presence of a binder-rich liquid phase and then precipitated on the surface of the coarse WC particles by migration, resulting in WC particle size growth. When the binder is added to the alloy, the contact area between the WC particles is reduced, thereby suppressing the interdiffusion of WC, resulting in limited growth of the WC particles. Furthermore, W dissolves in the binder phase during sintering, thereby suppressing W precipitation and WC grain growth. Consequently, the WC grains in the alloy become more uniform and finer.

Figure 10 shows a broken point sweep diagram of specimen WCN-6#. The binderless WC is difficult to reach a fully dense state due to the lack of a metal binder phase. In the present study, WC–Ni composite ceramics were obtained by vacuum pressureless sintering (VPS) followed by HIP sintering. Ni is added as a binder phase because its liquid exhibits good fluidity and wettability at high temperatures. As can be seen from Figure 10(a) and (b), the binder phase Ni distributed at the triple point of the grain boundary shows the characteristics of liquid phase sintering. The Ni phase melts into a liquid phase at a high temperature and penetrates the pores between the WC particles. It also penetrates the WC particles and is more closely aligned under the influence of the surface tension and capillary action of the WC particles, thereby promoting the densification of the sintering process [26]. The fluidity of liquid Ni increases with an increase in the temperature, and the driving force also increases, which accelerates the movement process of WC particles and thus increases the density of materials [3]. Moreover, the closed cells remaining after the VPS sintering can be eliminated by HIP, and a completely dense WC–Ni composite material is obtained. Simultaneous addition of grain growth inhibitors maintains the uniformity and fineness of the grains and also increases the density of the material.

4.2 Strengthening and toughening mechanisms

Figure 11 shows the line-cut method to calculate that the grain sizes of specimen WCN-5# and specimen WCN-6# are 0.64 and 0.74 μm, respectively, so that the specimens can be seen after VPS and HIP, and the grain size of WC did not grow significantly. During liquid phase sintering, small WC particles are premelted due to the presence of a binder-rich liquid phase between the WC particles and then precipitated on the surface of the coarse WC particles by migration, resulting in WC particle size growth. However, when the binder particles are added to the alloy, the contact area between the WC particles is reduced, thereby suppressing the interdiffusion of WC, resulting in limited growth of the WC particles. In addition, a small amount of grain inhibitors (VC and Cr_3C_2) are contained in the WC powder. It is found that the addition of VC and Cr_3C_2 grain inhibitors can effectively inhibit the growth of WC particles, reduce the size of WC particles, and control the abnormal growth of grains [53,54]. Results have shown that when too little VC and Cr_3C_2 are added or do not contain inhibitors, there are cases where the grains grow rapidly and grow abnormally. As the content of grain inhibitors increases, the grain size gradually decreases. The abnormal growth of the grain almost disappeared [12,45].

Figure 12 shows the fracture SEM results of specimens WCN-1#, WCN-2#, WCN-3#, WCN-4#, WCN-5#, and WCN-6#. A small number of small pores were observed on the fracture surface. The fracture modes of specimens

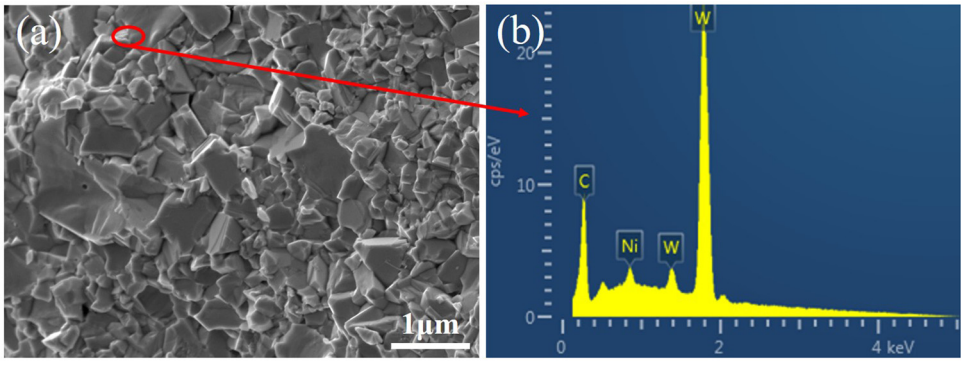

Figure 10: WCN-6# specimen fracture scanning and EDS results, (a) specimen fracture scanning, and (b) EDS results.

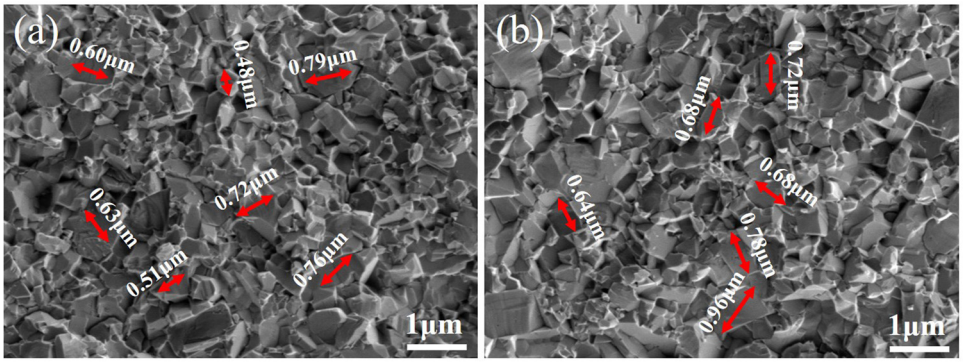

Figure 11: SEM images of (a) WCN-5# fracture and (b) WCN-6# fracture.

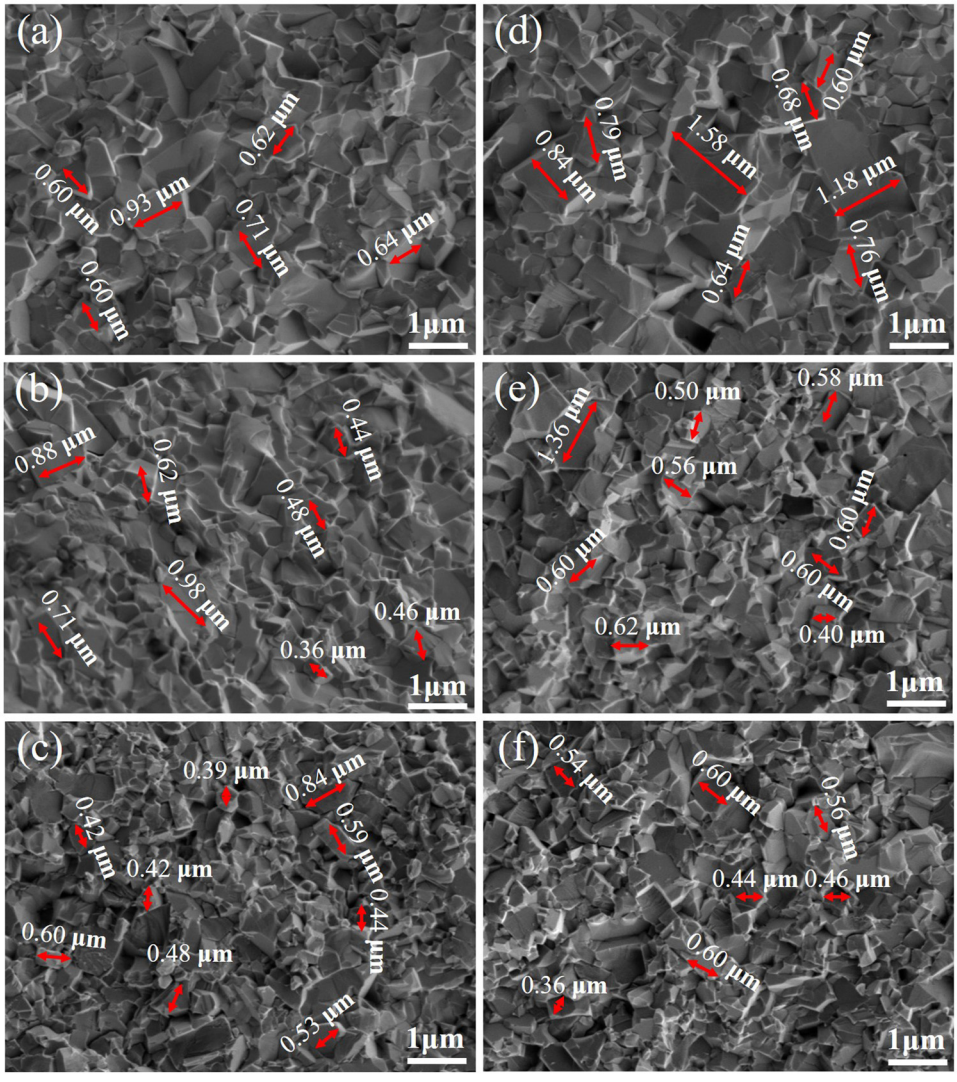

Figure 12: Fracture scanning: (a) WCN-1#, (b) WCN-2#, (c) WCN-3#, (d) WCN-4#, (e) WCN-5#, and (f) WCN-6#.

WCN-1# and WCN-2# were mainly the crystal fracture, while the specimens WCN-3–6# were mainly transgranular fracture. It was observed that the inner crystal grains of the material were planar, and there were few and very small wrapped inner holes. The reason is mainly because in the vacuum high-temperature sintering process, the degree of densification is mainly improved by the continuous migration of grain

boundaries and pores, and the contact between the powders is not tight due to uneven grinding and mixing between the raw material powders and diffusion driving during sintering. When the force is insufficient, the grain boundary migration speed is greater than the velocity of the pore migration, and the pores are generated. If the pores are to be eliminated, the pores are mainly diffused to the grain boundary by vacancies. Figure 12 shows that as the Ni content increases, the grain size of the WC–Ni composite ceramics gradually decreases. The reason may be the effect of VPS–HIP process technology after adding a small amount of binder. And at high temperatures, the powder can be fully contacted during a longtime sintering process and will generate sufficient diffusion driving force, thereby reducing the porosity. The reduction, and at the same time, the grain growth inhibitor component, hinders the abnormal growth of the WC particles, making the structure more uniform and dense, thereby improving the flexural strength of the composites. At the same time, the composites contain mainly the elongated triangular prism WC particles and Ni phase. The existence of nickel makes the fracture of the WC–Ni composite mostly of transgranular type with a small fraction of intergranular fracture mode, which can improve the flexural strength.

Figure 13 shows the fracture toughness indentation of the specimen WCN-6#. The brittle fracture occurs at the edge of the indentation and a slight deflection occurs at the crack. When the crack is deflected, the path increases and the crack propagation decreases. In this way, more energy increases the toughness of the composites. Comparing Figure 8 to analyze the effect of Ni content on the microstructure and mechanical properties of WC–Ni composite ceramics materials. Determine that the fracture mechanism is controlled by the Ni phase. When the WC–Ni composite ceramics is under pressure, the presence of the Ni phase will cause some micro-cracks in the WC–Ni composite ceramics, which in turn causes crack deflection, bridging and branch deflection, thereby improving the WC–Ni composite ceramics fracture toughness. At the same time, fracture toughness is also related to internal defects and grain size. It can be seen from the fracture observation of Figure 12 that the specimen WCN-1# has very low internal porosity and has high fracture toughness. According to the data analysis, the fracture toughness of the specimen WCN-1# was 5.76 MPa $m^{1/2}$.

5 Conclusions

In this work, the microstructure and properties of WC–Ni composite ceramics with WC–0.25 wt% Ni, WC–0.5 wt% Ni, and WC–1 wt% Ni were studied. The following results were obtained:

1. The addition of $NiCl_2{\cdot}6H_2O$ greatly reduces the difficulty of sintering WC–Ni composite ceramics. 0.5 wt% Ni was added to the WC matrix, and VPS at 1,560°C, followed by HIP at 1,600°C × 80 MPa × 1 h to obtain a fully dense WC–Ni composite ceramic.
2. TEM results show that the WC grains are lath or triangular, and there are dislocations, twins, and other dislocations in the interior. The distribution of the Ni phase in the composite is uniform. The grain growth inhibitors VC and Cr_3C_2 are mainly located at the crystal angle (edge) and facet interface of WC, which hinders the migration of grain boundaries, limits the growth of WC grains, and inhibits the abnormal growth of WC grains.
3. As the nickel content increases, the density gradually increases. When the nickel content increases to 1% of the mass fraction, the density decreases, because the liquid phase sintering is too long, resulting in a

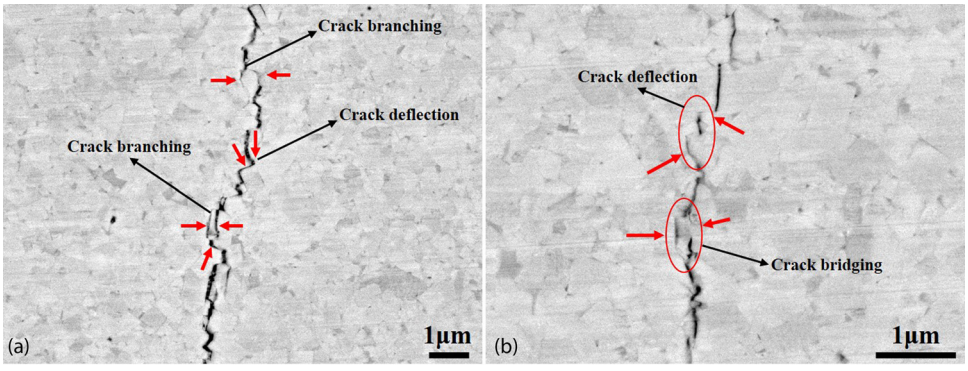

Figure 13: WCN-6# specimen: (a) fracture toughness indentation map and (b) partial enlarged view.

decrease in density. Specimen WCN-4# multiphase ceramics have a hardness of up to 23.0 GPa, a fracture toughness of 5.28 MPa $m^{1/2}$, and a flexural strength of 1396.58 MPa, and the WC grains remain fine and do not grow significantly.

4. The toughening mechanism of Ni to WC–Ni composite ceramics is due to microcracks, crack deflection, crack bridging, and crack bifurcation, which absorbs the energy of crack propagation, thereby increasing the surface area of crack propagation and increasing the fracture toughness of the composite.

Acknowledgments: This work was supported by Key Laboratory of Infrared Imaging Materials and Detectors, Shanghai Institute of Technical Physics, Chinese Academy of Sciences (No. IIMDKFJJ-19-08), and China Postdoctoral Science Foundation (No. 2015M570794 and 2018T110993).

Conflict of interest: The authors declare no conflict of interest regarding the publication of this paper.

References

[1] Yang Q, Yang J, Yang H, Ruan J. The effects of fine WC contents and temperature on the microstructure and mechanical properties of inhomogeneous WC-(fine WC–Co) cemented carbides. Ceram Int. 2016;42:18100–7.

[2] Zhou PL, Xiao DH, Zhou PF, Yuan TC. Microstructure and properties of ultrafine grained AlCrFeCoNi/WC cemented carbides. Ceram Int. 2018;44:17160–6.

[3] Ghasali E, Ebadzadeh T, Alizadeh M, Razavi M. Mechanical and microstructural properties of WC-based cermets: a comparative study on the effect of Ni and Mo binder phases. Ceram Int. 2018;44:2283–91.

[4] Wang X, Xu P, Han R, Ren J, Li L, Han N, et al. A review on the mechanical properties for thin film and block structure characterised by using nanoscratch test. Nanotechnol Rev. 2019;8:628–44.

[5] Sawicki K, Czajka M, Matysiak-Kucharek M, Fal B, et al. Toxicity of metallic nanoparticles in the central nervous system. Nanotechnol Rev. 2019;8:175–200.

[6] Kim HC, Shon IJ, Yoon JK, Doh JM, Munir ZA. Rapid sintering of ultrafine WC–Ni cermets. Int J Refract Met Hard Mater. 2006;24:427–31.

[7] Li S, Guo X, Zhang S, Feng J, Song K, Liang S. Arc erosion behavior of TiB_2/Cu composites with single-scale and dual-scale TiB_2 particles. Nanotechnol Rev. 2019;8(1):619–27.

[8] Balbino NAN, Correa EO, de Carvalho Valeriano L, Amâncio DA. Microstructure and mechanical properties of 90WC–8Ni–2Mo_2C cemented carbide developed by conventional powder metallurgy. Int J Refract Met Hard Mater. 2017;68:49–53.

[9] Li J, Cheng J, Chen P, Chen W, Wei C. Fabrication of WC-Co cemented carbides with gradient distribution of WC grain size and Co composition by lamination pressing and microwave sintering. Ceram Int. 2018;44:11225–32.

[10] Banerjee D, Huston WR, Zheng Q, Killman BJ. 2011, Wear resistant two-phase binderless tungsten carbide and method of making same, US patent 20110195834A1.

[11] Zhang J, Saeedm MH, Li S. Recent progress in development of high-performance tungsten carbide-based composites: synthesis, characterization, and potential applications. Adv Ceram Matrix Compos Second Ed. 2018;307–29.

[12] Poetschke J, Richter V, Holke R. Influence and effectivity of VC and Cr_3C_2 grain growth inhibitors on sintering of binderless tungsten carbide. Int J Refract Met Hard Mater. 2012;31:218–23.

[13] Almond EA, Roebuck B. Identification of optimum binder phase compositions for improved WC hard metals. Mater Sci Eng A. 1988;105–106:237–48.

[14] Chang SH, Chen SL. Characterization and properties of sintered WC–Co and WC–Ni–Fe hard metal alloys. J Alloys Compd. 2014;585:407–13.

[15] Jiang G, Zhuang H, Li W. Parameters investigation during simultaneous synthesis and densification WC–Ni composites by field-activated combustion. Mater Sci Eng A. 2003;360:377–84.

[16] Guo Z, Xiong J, Yang M, Jiang C. WC–TiC–Ni cemented carbide with enhanced properties. J Alloys Compd. 2008;465:157–62.

[17] Tang S, Li P, Liu D, Li P, Niu Q. Cutting performance of a functionally graded cemented carbide tool prepared by microwave heating and nitriding sintering. High Temp Mater Proc. 2019;38:582–9.

[18] Huang B, Chen LD, Bai SQ. Bulk ultrafine binderless WC prepared by spark plasma sintering. Scr Mater. 2006;54:441–5.

[19] Genga RM, Cornish LA, Akdogan G. Effect of Mo_2C additions on the properties of SPS manufactured WC–TiC–Ni cemented carbides. Int J Refract Met Hard Mater. 2013;41:12–21.

[20] Li ZH, Xu K, Pan YS. Recent development of supercapacitor electrode based on carbon materials. Nanotechnol Rev. 2019;8(1):35–49.

[21] Kwon HJ, Suh CY, Kim W. Microstructure and mechanical properties of (Ti,W)C–Ni cermet prepared using a nano-sized TiC–WC powder mixture. J Alloys Compd. 2015;639:21–26.

[22] Wan S, Bi HC, Sun L. Graphene and carbon-based nano-materials as highly efficient adsorbents for oils and organic solvents. Nanotechnol Rev. 2016;5(1):3–22.

[23] Gille G, Bredthauer J, Gries B, Mende B, Heinrich W. Advanced and new grades of WC and binder powder-their properties and application. Int J Refract Met Hard Mater. 2000;18(2–3):87–102.

[24] Chen HY, Wang ZC, Luo LM, Zhu L, Tu ZB, Wu YH. Effect of Ni content on microstructure and properties of WC–Ni composites prepared by electroless plating and powder metallurgy. Rare Met Mat Eng. 2017;46:2820–4.

[25] Garcia J. Influence of Fe–Ni–Co binder composition on nitridation of cemented carbides. Int J Refract Met Hard Mater. 2012;30(1):114–20.

[26] Lisovskii AF. Anomalous behavior of liquid metals in flat capillaries formed by sintered composite solids. Powder Metall Met C+. 1982;21(7):536–40.

[27] Engqvist H, Botton GA, Axén N, Hogmark S. A study of grain boundaries in a binderless cemented carbide. Int J Refract Met Hard Mater. 1998;16(4–6):309–13.
[28] Zhao ZY, Zhu DG, Gao Y, Lv L, Liao N, Jiang XS, et al. Influence of Ni and ZrO_2 contents on sintering and mechanical properties of WC–2 wt% ZrO_2–1 wt% Ni composites. Ceram Int. 2019;45:11241–50.
[29] Chen HS, Feng KQ, Xiong J, Luo JJ, Guo ZX, Wang H. Characterization and forming process of a functionally graded WC–Co/Ni composite. Int J Refract Met Hard Mater. 2012;35:306–10.
[30] Li J, Cheng J, Wei B, Chen P. Preparation and performance of ultrafine grained WC–10Co alloys with added La_2O_3. Ceram Int. 2019;45(3):3969–76.
[31] Pragatheeswaran A, Ravi R, Bakshi SR. Microstructural and morphological changes during ball milling of copper–silver–graphite flake mixtures. Adv Powder Technol. 2019;30(11):2759–67.
[32] Li R, Gong L, Lin J, Wang K, Shi Z. Structural evolution of Fe–Y2O3–Ti powder during ball-milling and thermal treatment. Ceram Int. 2019;45(16):20011–5.
[33] Taimatsu H, Sugiyama S, Kodaira Y. Synthesis of W_2C by reactive hot pressing and its mechanical properties. Mater Trans. 2008;49(6):1256–61.
[34] Cha SI, Hong SH. Microstructures of binderless tungsten carbides sintered by spark plasma sintering process. Mater Sci Eng A. 2003;356(1–2):381–9.
[35] Hartmann C, Wollweber J, Sintonen S, Dittmar A, Kirste L, Kollowa S, et al. Preparation of deep UV transparent AlN substrates with high structural perfection for optoelectronic devices. CrystEngComm. 2016;18:3488–97.
[36] Nokhrin AV, Chuvil'deev VN, Boldin MS, Piskunov AV, Kozlova NA, Chegurov MK, et al. The use of spark plasma sintering method for high-rate diffusion welding of high-strength UFG titanium alloys. IOP Conf Ser: Mater Sci Eng. 2017;218(1):12013.
[37] Raekelboom E, Abdelouahdi K, Legrand-Buscema C. Structural investigation by the rietveld method of sputtered tungsten carbide thin films. Thin Solid Films. 2009;517(5):1555–8.
[38] Shatov AV, Firstov SA, Shatova IV. The shape of WC crystals in cemented carbides. Mater Sci Eng A. 1998;242(1–2):7–14.
[39] Mukhopadhyay A, Basu B. Recent developments on WC-based bulk composites. J Mater Sci. 2011;46(3):571–89.
[40] Kim HC, Shon IJ, Garay JE, Munir ZA. Consolidation and properties of binderless sub-micron tungsten carbide by field-activated sintering. Int J Refract Met Hard Mater. 2004;22(6):257–64.
[41] Kim HC, Kim DK, Woo KD, Ko IY, Shon IJ. Consolidation of binderless WC–TiC by high frequency induction heating sintering. Int J Refract Met Hard Mater. 2008;26(1):48–54.
[42] Liu XW, Song XY, Wang HB, Liu XM, Wang XL, Guo GS. Preparation and mechanisms of cemented carbides with ultrahigh fracture strength. J Appl Crystallogr. 2015;48(4):1254–63.
[43] Lee SB, Yoon DY, Henry MF. Abnormal grain growth and grain boundary faceting in a model Ni-base superalloy. Acta Mater. 2000;48(12):3071–80.
[44] Lay S, Hamar-Thibault S, Lackner A. Location of VC in VC, Cr_3C_2 codoped WC–Co cermets by HREM and EELS. Int J Refract Met Hard Mater. 2002;20(1):61–69.
[45] Dong WW, Zhu SG, Wang Y, Bai T. Influence of VC and Cr_3C_2 as grain growth inhibitors on WC–Al_2O_3 composites prepared by hot press sintering. Int J Refract Met Hard Mater. 2014;45:223–9.
[46] Franco E, da Costa CE, Tsipas SA, Gordo E. Cermets based on FeAl–NbC from composite powders: design of composition and processing. Int J Refract Met Hard Mater. 2015;48:324–32.
[47] Lisovsky AF. The thermodynamics of the liquid phase migration in nanodispersed composite bodies. Int J Heat Mass Transf. 2009;52(21–22):4766–8.
[48] Chang SH, Chang MH, Huang KT. Study on the sintered characteristics and properties of nanostructured WC–15 wt% (Fe–Ni–Co) and WC–15 wt% Co hard metal alloys. J Alloys Compd. 2015;649:89–95.
[49] Huang SG, Vanmeensel K, Van der Biest O, Vleugels J. Binderless WC and WC–VC materials obtained by pulsed electric current sintering. Int J Refract Met Hard Mater. 2008;26(1):41–7.
[50] Cheng JG, Wu YC, Xia YH. Fabrication of WC–Co cemented carbides with gradient distribution of WC grain size and Co composition by tape casting. Mater Sci Forum. 2003;423–425:45–8.
[51] Kumar A, Singh K, Pandey OP. Sintering behavior of nanostructured WC–Co composite. Ceram Int. 2011;37(4):1415–22.
[52] Chang SH, Lu CW, Chen JK. Study on the microstructures, electrical resistance and mechanical properties of sputtering chromium target by HP, HIP and canning – HIP processes. Int J Refract Met Hard Mater. 2012;35:70–75.
[53] Wang Y, Zhu DG, Jiang XS, Sun PQ. Binderless sub-micron WC consolidated by hot pressing and treated by hot isostatic pressing. J Ceram Soc Jpn. 2014;122(1425):329–35.
[54] Sun L, Yang TE, Jia CC, Xiong J. VC, Cr_3C_2 doped ultrafine WC–Co cemented carbides prepared by spark plasma sintering. Int J Refract Met Hard Mater. 2011;29(2):147–52.